International Journal of Applied Earth Observations and Geoinformation 96 (2021) 102260

Contents lists available at ScienceDirect

International Journal of Applied Earth Observations and Geoinformation

journal homepage: www.elsevier.com/locate/jag

Fusion of Sentinel-2 and PlanetScope time-series data into daily 3 m surface reflectance and wheat LAI monitoring

Yuval Sadeh [a,*], Xuan Zhu [a], David Dunkerley [a], Jeffrey P. Walker [b], Yuxi Zhang [b], Offer Rozenstein [c], V.S. Manivasagam [c,d], Karine Chenu [e]

[a] School of Earth, Atmosphere and Environment, Monash University, Clayton, Victoria 3800, Australia
[b] Department of Civil Engineering, Monash University, Clayton, Victoria 3800, Australia
[c] Institute of Soil, Water and Environmental Sciences, Agricultural Research Organization, Volcani Center, Rishon LeZion 7528809, Israel
[d] Amrita School of Agricultural Sciences, Amrita Vishwa Vidyapeetham, J. P. Nagar, Arasampalayam, Myleripalayam, Coimbatore - 642 109, Tamil Nadu, India
[e] Queensland Alliance for Agriculture and Food Innovation, The University of Queensland, 13 Holberton street, Toowoomba, Queensland 4350, Australia

ARTICLE INFO

Keywords:
Leaf area index
CubeSat
Data fusion
Crop monitoring
Vegetation indices
Time series

ABSTRACT

The dynamics of Leaf Area Index (LAI) from space is key to identify crop types and their phenology over large areas, and to characterize spatial variations within growers' fields. However, for years remote-sensing applications have been constrained by a trade-off between the spatial and temporal resolutions. This study resolves this limitation. Over the past decade, the number of companies and organizations developing CubeSat constellations has increased. These new satellites make it possible to acquire large image collections at high spatial and temporal resolutions at a relatively low cost. However, the images obtained from CubeSat constellations frequently suffer from inconsistency in the data calibration between the different satellites within the constellation. To overcome these inconsistencies, a new method to fuse a time series of images sourced from two different satellite constellations is proposed, combining the advantages of both (i.e., the temporal, spatial and spectral resolution). This new technique was applied to fuse PlanetScope images with Sentinel-2 images, to create spectrally-consistent daily images of wheat LAI at a 3 m resolution. The daily 3 m LAI estimations were compared with 57 *in-situ* wheat LAI measurements taken in Australia and Israel. This approach was demonstrated to successfully estimate Green LAI (LAI before the major on-set of leaf senescence) with an R^2 of 0.94 and 86% relative accuracy (RMSE of 1.37) throughout the growing season without using any ground calibration. However, both the Sentinel-2 based estimates and the fused Green LAI were underestimated at high LAI values (LAI > 3). To account for this, regression models were developed, improving the relative accuracy of the Green LAI estimations by up to a further 47% (RMSE of 0.35–0.63) in comparison with field measured LAI. The new time series fusion method is an effective tool for continuous daily monitoring of crops at high-resolution over large scales, which opens up a range of new precision agriculture applications. These high spatio-temporal resolution time-series are valuable for monitoring crop growth and health, and can improve the effectiveness of farming practices and enhance yield forecasts at the field and sub-field scales.

1. Introduction

Improving the spatial and temporal estimation of Leaf Area Index (LAI) and monitoring of the crop developmental stage using remotely sensed imagery can inform service providers and growers to facilitate management decisions, formulate policies, and ultimately improve profitability (Pasqualotto et al., 2019; Sun et al., 2019). LAI also plays an important role in crop monitoring and can be used in crop growth models to better predict yield (Bøgh et al., 2004; Clevers, 1991; Lobell et al., 2015). One of the common applications for LAI is to provide yield estimations (e.g. Azzari et al., 2017; Ines et al., 2013; Lobell et al., 2015; Sun et al., 2017; Waldner et al., 2019).

LAI is defined as the ratio of one-sided leaf area per unit ground area (Watson, 1947) and knowing the LAI of a crop has a wide range of applications. However, monitoring crop LAI by extensive *in-situ* sampling over large areas is expensive, time consuming and consequently impractical (Houborg and McCabe, 2018c). Therefore, for decades scientists around the world have attempted to estimate LAI from space (e.g.

* Corresponding author.
E-mail address: yuval.sadeh@monash.edu (Y. Sadeh).

https://doi.org/10.1016/j.jag.2020.102260
Received 11 May 2020; Received in revised form 7 September 2020; Accepted 22 October 2020
Available online 16 November 2020

Chen et al., 2002; Gitelson et al., 2003; Nguy-Robertson et al., 2014; Pollock and Kanemasu, 1979; Viña et al., 2011; Wiegand et al., 1979). However, the trade-off between the spatial and temporal resolution typically restricted the use of high spatial and temporal time-series of images for agricultural applications (Waldner et al., 2019).

As crop canopy reflectance is affected by the LAI, as well as by the chlorophyll distribution, canopy structure and the background soil (Gitelson et al., 2005), methods which rely on optical remote sensing to convert surface reflectance data into LAI estimations were developed (Delegido et al., 2015). These methods are commonly classified into two groups (Delegido et al., 2015; Fang et al., 2019; Kimm et al., 2020; Pasqualotto et al., 2019): (i) physically-based retrieval methods, which are based on radiative transfer models (RTM), when the LAI is estimated based on the inversion of these models (e.g. Houborg and McCabe, 2018c), and (ii) an empirical approach using either linear or nonlinear regressions with vegetation indices (VIs) as independent variables (e.g. Herrmann et al., 2011; Nguy-Robertson et al., 2014). These two groups of methods have both advantages and disadvantages. The physically-based retrieval methods are more generally applicable, but they are often limited by the nature of canopy structure and thus suffer from the ill-posed problem that may end in an unstable solution and require an a priori knowledge of targeted canopies (Bsaibes et al., 2009; Delegido et al., 2015). The empirical methods are commonly based on pre-trained relationships between field measured LAI and VIs; they are simple and do not require intensive computation. However, these empirical relationships could only be useful in regions that are similar to those used for calibration (Bsaibes et al., 2009; Kimm et al., 2020) and are less reliably applied for multiple vegetation types (Pasqualotto et al., 2019).

The majority of these methods have been developed for retrieving LAI from green vegetation only (Delegido et al., 2015), which is often called the Green Leaf Area Index (Green LAI or LAI-green). The Green LAI represents the leaves which are photosynthetically active (Daughtry et al., 1992). In contrast to the brown or senescing LAI (Delegido et al., 2015), remotely sensed Green LAI is more useful for agro-ecosystem monitoring (Pasqualotto et al., 2019), assessment of water logging damage in agriculture (Liu et al., 2018), estimating vegetation phenology (Verger et al., 2016), monitoring of deforestation (Valderrama-Landeros et al., 2016), crop modelling (El Hajj et al., 2016) and yield prediction (Lobell et al., 2015).

Previous studies showed that LAI can be estimated using spaceborne sensors such as AVHRR (Franch et al., 2017), MODIS (Huang et al., 2015), Landsat (Gao et al., 2012), WorldView-2 (Psomiadis et al., 2017) and Sentinel-2 (S2) (Djamai et al., 2019; Pasqualotto et al., 2019; Verrelst et al., 2015). Each of these sensors has their pros and cons, which mainly arise from their spatial, temporal and spectral resolutions or costs. Over the last decade, the number of companies developing CubeSats has increased. These new satellites, such as Planet Labs' PlanetScope (PS) CubeSat, can be the size of a milk carton, are relatively inexpensive to build and launch to a low earth orbit, thereby making it possible to acquire large image collections at high spatial and temporal resolutions at a relatively low cost. However, one of the major challenges working with time series CubeSat imagery is the fact that unlike large and expensive satellites such as S2 or Landsat, the images obtained from CubeSat constellations, such as Planet's PS, frequently suffer from radiometric inconsistencies in the data collected by the different satellites within the constellation, due to inter-calibration challenges and their low signal-to-noise ratio (Houborg and McCabe, 2016, 2018b; Leach et al., 2019; Sadeh et al., 2019).

The lack of suitable combinations of both high spatial and temporal resolution time series from well calibrated satellite images (Waldner et al., 2019) motivated a few attempts to fuse CubeSat imagery with these other types of imagery into high spatio-temporal LAI datasets. For example, Houborg and McCabe (2018b) created Landsat-consistent LAI of an irrigated alfalfa field in Saudi Arabia by fusing PS, Landsat and MODIS images coupled with *in-situ* measurements, to spatially and temporally enhance Landsat-based LAI to the PlanetScope resolution. Li et al., (2019) generated red-edge bands at 3 m spatial resolution by fusing S2 and PS images, by using the weight-and-unmixing algorithm as well as the SUPer-REsolution for multi-spectral Multi-resolution Estimation (Wu-SupReME) approach. However, their fusion method was tested with only a few individual images acquired on selected dates, and their relationship between *in-situ* wheat LAI measurements and the VIs from fused images only applies to Jiangsu Province, China, where it was established. Kimm et al., (2020) used the Moderate Resolution Imaging Spectroradiometer (MODIS)-Landsat STAIR (SaTellite dAta IntegRation) fusion product (Luo et al., 2018) and fused it with PS data to produce daily LAI estimation of corn and soybean in the U.S. Corn Belt. The STAIR method uses an adaptive-average correction that takes into account different land cover types through an automatic segmentation of the image (Luo et al., 2018).

Motivated by the inconsistency issues of the data acquired by the different satellites within the constellation, this study: 1) proposed a new method to fuse time series of images sourced from two different satellites to overcome the inconsistencies between the different sensors within the CubeSat constellation, and combines the advantages of both data sources in terms of their temporal, spatial and spectral resolutions. In contrast to some other fusion methods (e.g. Gao et al., 2006; Li et al., 2019), which can take only one or two pairs of images as input at a time, this new method can process a time series from an unlimited number of images; 2) applied this new technique to fuse PS images (with a spatial resolution of ~3 m, and a daily revisit time) and S2 images (resolution of 10 m and five-day revisit time) to create daily, S2-consistent surface reflectance blue, green, red (visible) and near-infrared (NIR) and crop Green LAI at a 3 m resolution; 3) tested the approach for improved wheat LAI estimation over wheat fields in Australia and Israel, so as to provide an assessment over different soil types, farm management, climates and crop varieties. The guideline for the development of the method was that the method should be simple, so it could be easily be replicated and applied elsewhere. Therefore, the reliable and well-studied Sentinel-2 LAI product was selected, which offer a global coverage of LAI estimates in a relatively high spatial resolution. Recently developed methods for LAI estimation tend to use sophisticated computing techniques such as machine learning, but they typically involve the use of ground-based training data specific to the study area. This paper contends that a practical and robust method for LAI estimation should be simple, effective, repeatable and universal. Therefore, the Sentinel-2 LAI product was selected as the reference, having global coverage of LAI estimates at relatively high spatial resolution. By converting the fused VIs into Sentinel-2-like LAI estimates (as described in Section 2.4), the need of having ground LAI data is unnecessary. The resulting daily 3 m LAI estimations were compared with *in-situ* wheat LAI measurements made using ground-based methods. This new time series fusion method facilitates continuous daily high-resolution monitoring of crops over large scales.

2. Methods

2.1. Field trials and in-situ LAI measurements

2.1.1. Cora Lynn trial

Winter-wheat variety RGT Accroc was grown in a 76 × 74 m field 80 km South-East of Melbourne, Victoria, Australia, at Cora Lynn (38.1336° S, 145.6324° W, average annual rainfall of 857 mm (Australian Bureau of Meteorology, 2020)). The crop was sown in the silty loam at a 5 cm depth on Aug 7, 2018, with 100 kg ha-1 MAP (mono-ammonium phosphate) applied at sowing. The crop was grown under rainfed conditions, with only one irrigation (Nov 16, 2018) of 50 m^3 ha^{-1} with a linear shift irrigator, to avoid plant death. Four sets of above-ground plant parts were collected from the four sides of the field (at least 2 m from the edge) 16 times during the growing season, in a 0.5 × 0.5 m sampling area. For one or two of those four sets, leaf blades, stems and sheaths, and heads were portioned to measure their dry biomass and

calculate the proportion of leaf material (i.e., dry weight of the blades divided by the total above-ground biomass). A subset of approximately 100 blades from the sampled leaves were then scanned using a Canon imageRUNNER ADVANCE C3330 scanner (Canon Inc) and weighed, after oven dry at 60 °C for at least 48 h, to measure the specific leaf area. LAI was calculated by multiplying specific leaf area, the proportion of leaf in the subsample and the average biomass of four samples, and by dividing by the sampling area.

2.1.2. Birchip fields

Five rainfed spring-wheat fields were studied in a farm located near Birchip, Victoria, Australia (Apr-Nov 2018; 35.982° S, 142.916° W), representing an average Victorian farm in the Australian wheat belt. The Birchip farm, which, is 6,400 ha in size (average field size is 116 ha), was chosen for this study as it represents a typical Australian rainfed crop farm. This site is located on fine sandy clay loam texture soil and receives an average annual rainfall of 374 mm (Australian Bureau of Meteorology, 2020). The LAI measurements were conducted on the 17th and 18th of September 2018 using a LAI-2000 Plant Canopy Analyzer (LI-COR). Ten 20 m × 20 m plots located in five wheat fields were selected (two in each field). All plots were located at least 20 m away from the edges of the field and were representative of the crops' conditions in their area. Field data were acquired following the measurement guidelines suggested by the instrument manual (LI-COR, 1992). In total, 240 individual LAI measurements were sampled for the ten plots, with each plot containing 24 LAI measurements.

2.1.3. Saad and Yavne fields

LAI was measured over six rainfed spring-wheat fields, located in two commercial farms near Saad (four fields of ~ 39 ha in total; Feb-Apr 2018; 31.477° N, 34.538° W) and Yavne (two fields of ~ 13 ha in total; Jan-Apr 2019; 31.809° S, 34.716° W) in Israel. The Saad fields are located over a clay soil and receive an average annual rainfall of 415 mm (Israel Meteorological Service, 2020). The Yavne fields are located over a sandy loam soil and receive an average annual rainfall of 515 mm (Israel Meteorological Service, 2020). LAI in these two sites was measured using the SunScan Canopy Analysis System (SS1-COM-R4 Complete System with Radio Link developed by Delta-T Company, Cambridge, United Kingdom). The four fields in Saad were close to each other with different sowing dates and irrigation regimes: Kitain cv sown on 20/11/2017 and grown under both rainfed (1) and with some irrigation (2); Amit cv was sown on 29/11/2017 and grown under rainfed conditions (3), and durum wheat cultivar C9 was sown on 19/11/2017 and grown under rainfed conditions. The two fields in Yavne were adjacent and sown on 16/11/2018. The measurements performed six times for the Saad farm fields and seven times for the Yavne farm fields during the growing season. Each LAI value used for the analyses was the average of LAI measured at 2 to 4 points, separated to each other by a distance of ~50 m. At each point, around 30 field measurements were taken every ~20 cm from each other, regardless of whether plants were present or not.

2.2. Imagery

2.2.1. Sentinel-2 (surface reflectance and LAI)

The European Space Agency (ESA) Copernicus Sentinel-2 (S2) includes a constellation of two polar-orbiting satellites positioned in the same sun-synchronous orbit, but phased at 180° to each other. S2 carries an optical sensor payload that samples 13 spectral bands: four bands at 10 m, six bands at 20 m and three bands at 60 m spatial resolution. It provides a revisit frequency of 5 days (at the Equator) with a 290 km swath width (Drusch et al., 2012; SUHET, 2015). S2 images can be freely downloaded at the Copernicus Open Access Hub website (https://scihub.copernicus.eu/dhus/#/home). In this study, clear-sky images downloaded via ESA's application programming interface (API), using the field's polygon to determine the region of interest (ROI) to be downloaded. S2 Level-2A Bottom Of Atmosphere (BOA) products were only available (and used) for Israel during the study period. For Australia, we thus used the Sen2Cor module (Louis et al., 2016) within ESA's Sentinel Application Platform (SNAP) software (version 7.0) to convert the Level-1C product (Top Of Atmosphere (TOA) reflectance) images from TOA to BOA, in order to minimize the influence of the atmospheric conditions present at the time of acquisition. Next, S2-based LAI data (from Israel and Australia) were generated using the Biophysical Processor module embedded in SNAP, which computes biophysical products from S2 BOA reflectance. This processor uses the top-of-canopy reflectance data to estimate a number of biophysical variables including LAI (Weiss and Baret, 2016).

2.2.2. PlanetScope

PlanetScope (PS) is a CubeSat 3U form factor (10 cm × 10 cm × 30 cm) satellite constellation operated by Planet Labs, Inc. The PlanetScope constellation consists of about 120 satellites, with the capability to image all of the Earth's land surface on a daily basis. The PlanetScope satellites have four spectral bands; Blue (455–515 nm), Green (500–590 nm), Red (590–670 nm) and NIR (780–860 nm). These have a Ground Sampling Distance (GSD) of 3–4 m at nadir and a positional accuracy of <10 m RMSE (Planet Team, 2018). This study used the Planet Surface Reflectance Product provided at a spatial resolution of ~3 m. These images are atmospherically corrected to BOA reflectance, which provides more consistency across time and location localized atmospheric conditions while minimizing uncertainty in the spectral response (Planet Team, 2020). Despite the fact that both PS and S2 provide imagery in the visible and NIR regions, their bandwidths and spectral response are very different as shown in Fig. 1. For each analysed field, cloud-free PlanetScope images were downloaded using Planet's API, according to the field's domain.

2.3. Data fusion of reflectance

In order to fuse images acquired by the PS CubeSats constellation and S2, we have developed a simple fusion method (Fig. 2). The data fusion process required four inputs: (1) High spatio-temporal resolution images (e.g. PS); (2) lower spatial resolution, but with higher spectral resolution images (e.g. S2); (3) an index or product produced by input number 2 (e.g. LAI); and 4) the ROI (i.e., a polygon of field's domain). The outputs of this fusion method are daily fused surface reflectance images and daily images of the desired index or product, in the original pixel size of the high spatial resolution input. In this study, we tested our fusion method to produce S2-like visible-NIR bands and LAI images at the spatial and temporal resolution of PS (i.e., daily images in 3 m).

First, PS, S2 (bands 2, 3, 4 & 8) and S2-based LAI images were extracted by the field's domain. Then, each type of consecutive pair of images acquired at two different dates are linearly interpolated to create a daily time-series of images. This results in three separate time-series, (1) PS BOA (3 m), (2) S2 BOA (10 m), and (3) S2 LAI (10 m) made from both real as well as synthetic (interpolated) images. Next, the S2-based datasets (2 + 3) were resampled (using cubic interpolation) from 10 m to 3 m pixel size. Then, same-day PS and the resized S2 images are separated into their individual bands (Blue, Green, Red and NIR), and fused by averaging the pixel values between each pair of bands as follow:

$$\text{Fused Band}_i = (\text{PlanetScope}_{\text{BOA}}\text{Band}_i + \text{Sentinel2}_{\text{BOA}}\text{Band}_i)/2 \quad (1)$$

where Band_i correspond to each of RGB visible and the NIR bands (Fig. 1). After the fusion, the bands are recombined to form an RGB-NIR image. This stage yields in daily 3 m fused surface reflectance images.

2.4. Fused LAI in 3 m

The new dataset is then used to calculate 13 selected vegetation

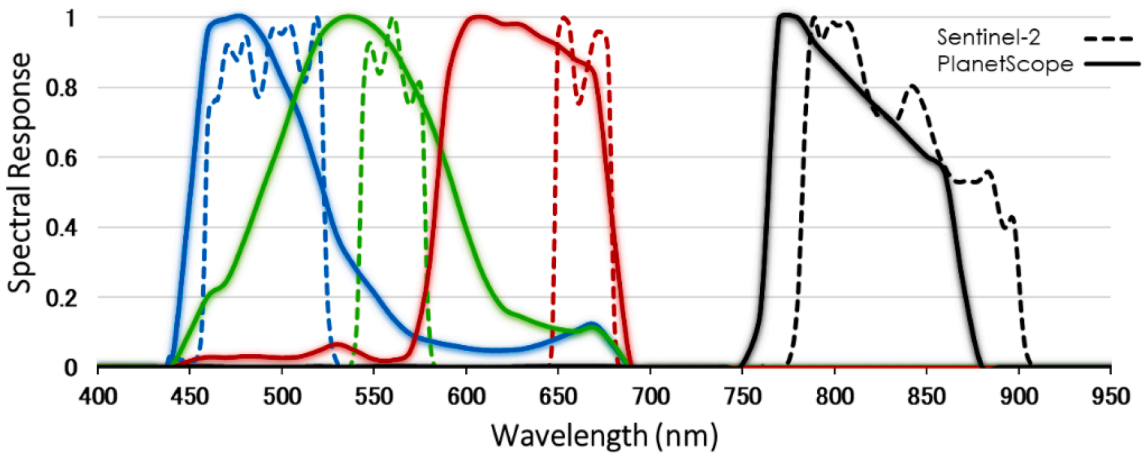

Fig. 1. The spectral response of Sentinel-2 and PlanetScope in the Blue, Green, Red and Infrared bands.

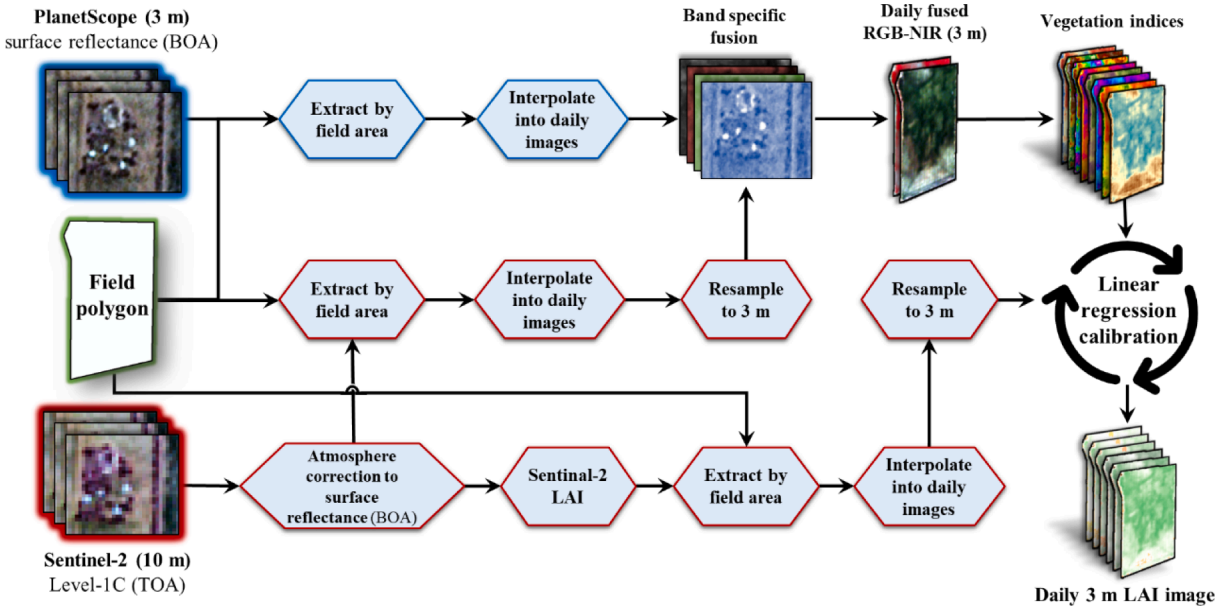

Fig. 2. The data fusion workflow of PlanetScope (with a spatial resolution of ~3 m) and Sentinel-2 (10 m) imagery into daily surface reflectance images, vegetation indices and LAI maps with a 3 m resolution.

indices shown in the literature to have a high correlation with LAI: SR, EVI2, NDVI, GCVI, MTVI2, MSAVI, WDRVI, Green-WDRVI, OSAVI, GSR, GNDVI, RDVI and TVI (Table 1). Finally, the vegetation indices from the fused image (daily, 3 m) are converted to LAI using a linear regression between the different vegetation indices to the resized LAI time-series (daily, 3 m) from S2. A four-day moving window (t_0, t_{-1}, t_{-2}, &t_{-3}) with same day (t_0) pairs of S2-LAI and a fused vegetation index image, was used to calculate the average slopes and intercepts between all four pairs (i.e., S2-LAI and one of the fused-based vegetation indices at the time). In this process, the slope and intercept of LAI and VI for all pixels from the field was calculated for each day and each studied vegetation index, and then averaged across the four days of the moving-window. Hence for each vegetation index, the correction of each image is done using a different slope and intercept, calculated for each four-day window, thus operating as a moving average. This was done in order to minimise the signal inconsistency created by the PS sensors (daily measurements), which causes variability in the vegetation indices. The algorithm was designed to use the last four days so it can work in operational near real-time mode, as the future images are still not available. However, when processing an existing time series of images, the algorithm can be easily be modified to include the next images in the time series (e.g., t_{-2},t_{-1},t_0,t_1,t_2,). The following equation is then used to correct and generate the daily high spatio-temporal LAI dataset:

$$Corrected\ image = Fused\ vegetation\ index^{*}four\text{-}day\ window\ slopes\ average + four\text{-}day\ window\ intercepts\ average \quad (2)$$

This method (Fig. 2) enables daily 3 m LAI images to be generated at

Table 1
Definition of the multispectral vegetation indices investigated in this study.

Vegetation index	Equation	Reference
Simple Ratio (SR)	$\frac{NIR}{Red}$	Jordan (1969)
Enhanced Vegetation Index 2 (EVI2)	$\frac{2.5(NIR - Red)}{(NIR + 2.4Red + 1)}$	Jiang et al. (2008); Nguy-Robertson et al. (2012)
Green Chlorophyll Vegetation Index (GCVI)	$(NIR - Green) - 1$	Gitelson et al. (2003); Gitelson et al. (2005)
Normalized Difference Vegetation Index (NDVI)	$\frac{NIR - Red}{NIR + Red}$	Rouse et al. (1974)
Modified Triangular Vegetation Index 2 (MTVI2)	$\frac{1.5[1.2(NIR - Green) - 2.5(Red - Green)]}{\sqrt{(2NIR + 1)^2 - (6NIR - 5\sqrt{Red}) - 0.5}}$	Haboudane et al. (2004)
Modified Soil-Adjusted Vegetation Index (MSAVI)	$0.5\left[2NIR + 1 - \sqrt{(2NIR + 1)^2 - 8(NIR - Red)}\right]$	Haboudane et al. (2004); Qi et al. (1994)
Wide Dynamic Range Vegetation Index (WDRVI)	$\frac{\alpha \cdot NIR - Red}{\alpha \cdot NIR + Red} + \frac{1 - \alpha}{1 + \alpha}$	Gitelson (2004); Nguy-Robertson et al. (2014)
Green Wide Dynamic Range Vegetation Index (Green-WDRVI)	$\frac{\alpha \cdot NIR - Green}{\alpha \cdot NIR + Green} + \frac{1 - \alpha}{1 + \alpha}$	Nguy-Robertson et al. (2014); Peng and Gitelson (2011)
Optimized Soil-Adjusted Vegetation Index (OSAVI)	$\frac{NIR - Red}{NIR + Red + 0.16}$	Rondeaux et al. (1996)
Green Simple Ratio (GSR)	$\frac{NIR}{Green}$	Sripada et al. (2006)
Green NDVI (GNDVI)	$\frac{NIR - Green}{NIR + Green}$	Gitelson and Merzlyak (1994)
Renormalized Difference Vegetation Index (RDVI)	$\frac{NIR - Red}{\sqrt{NIR + Red}}$	Roujean and Breon (1995)
Transformed Vegetative Index (TVI)	$\sqrt{\frac{NIR - Red}{NIR + Red} + 0.5}$	Rouse et al. (1974) Haas et al. (1975)

*α in WDRVI and Green-WDRVI = 0.1 following Nguy-Robertson et al. (2014).

the same quality as the S2 LAI product.

The remotely sensed LAI estimates were validated against the *in-situ* measurements. As the LAI was measured using different approaches over different study areas, the accuracy of the remotely sensed Green LAI was evaluated using a 23 × 23 square metre plot and a 65 × 65 square metre plot for the Birchip and Cora Lynn sites respectively. The fields in Israel were compared at the field level as each LAI measurement point was about 50 m apart from each other, and around 30 field measurements were taken at each of these points. The fields near Saad (four fields of ~39 ha in total) and Yavne (two fields of ~13 ha in total) are much smaller than the Australian commercial fields analysed in this study (the average field size is 116 ha) and the development of the crops in these fields has been far more homogeneous.

2.5. Adjustment of remotely-sensed Green LAI

The Green LAI (representing a canopy mostly photosynthetically active) are difficult to measure from space when leaves shade each other. To account for this, the Green LAI estimations were tested for improvement by adjusting the generic S2-LAI product estimations, to better estimates wheat Green LAI. This was done by 'fine-tuning' the results received in the previous stage, using second-order polynomial regressions (Table 4), which was found to best represent the correlation between the *in-situ* and remotely estimated Green LAI for a considered vegetation index. The performance of this correction approach was tested using an independent dataset of Green LAI for two ~30 ha, rainfed-wheat fields located near Yanco, NSW, Australia (Apr-Nov 2019; 34.716° S, 146.088° W). In this site, located more than 350 km from the nearest field used for training (i.e., further than the distance between Paris and London), the LAI was measured weekly using LI-COR LAI-2200 sensor during one month around the peak LAI (Oct 2019). The LAI measurements were taken at least 10 m away from the edges of the field and were representative of the crops' conditions in their area. Owing to the high spatial variability of the vegetation development in these two fields, the validation between the *in-situ* and the remotely sensed LAI performed on the crops located around the actual location of the LAI measurements (using a 0.3 and 0.4 ha plots). The results of the corrected Green LAI were compared with the *in-situ* Green LAI measurements and the non-corrected estimations, in order to validate the proposed correction method to better estimate wheat Green LAI from space.

3. Results

3.1. Fused surface reflectance accuracy

The implementation of the new fusion method to generate time series of images resulted in a new dataset, which maintained both the high spatial and temporal resolution of PS and the spectral quality of S2 (Figs. 3 and 4). Fig. 3 illustrates how a 10 m image from S2 fails to provide information about objects smaller than 10 m such as buildings, trees, and roads. By contrast, the fused image enabled easy identification of objects that could not be recognized in the S2 image while preserving the S2 reflectance information as shown in Fig. 4.

The correlation between the BOA surface reflectance of S2, PS and the fused images was compared and evaluated at the pixel level, while excluding 15 m from the fields' edges to avoid having mixed pixels with the surrounding objects. The mean and median R^2 across all bands for the studied PS and S2 images were only 0.6 and 0.7, respectively (Table 2). The highest correlations were found in the NIR wavelength (0.75 and 0.81 mean and median, respectively), while the lowest correlation was found in the blue wavelength (0.46 and 0.53 mean and median, respectively). The fused images were found to be highly correlated with the S2 images in all four bands (0.88 and 0.94 mean and median, respectively), being slightly higher than the correlation found between the fused images and PS images (0.84 and 0.9 mean and median, respectively). Sometimes when small objects such as scattered trees were located within the field, the analysis showed scattered pixels with lower correlation (Fig. 4). This is often because the lower resolution of S2 tends to represent these objects as mixed pixels, while they can be clearly identified in the fused image.

3.2. Fused vegetation indices

The ability of the fused images to produce daily vegetation indices (VIs) time-series in values similar to S2-based time-series was tested and compared to both VIs derived from S2 and PS. Overall, it was found that PS-based VIs tended to have lower values than S2-based VIs except in the early stages of the growing season (e.g., on low VIs values) where PS-based VIs were slightly higher (e.g., Fig. 5). Furthermore, a time-series of VIs generated based on PS images were noisier than the one generated based on S2 images or fused images (e.g., Fig. 5).

After fusing the S2 and PS images and calculating the VIs, daily 3 m LAI maps were generated (Fig. 6). These maps were compared to S2-

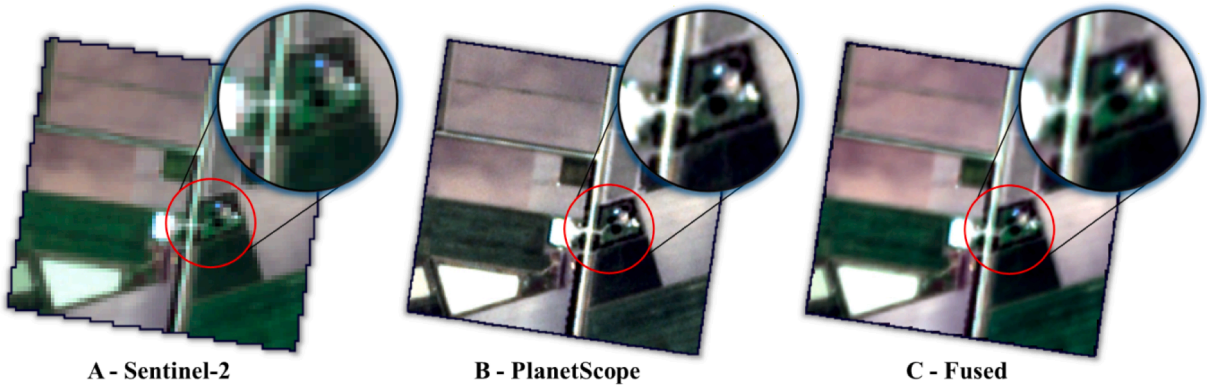

Fig. 3. An example of the Sentinel-2 and PlanetScope fusion outcome (in natural color composite image) for the Cora Lynn experimental field area. Both source images were acquired on the 29/9/18 and are in BOA reflectance values. (A) The original Sentinel-2 image (10 m), (B) the original PlanetScope image (3 m), and (C) the fused image (3 m).

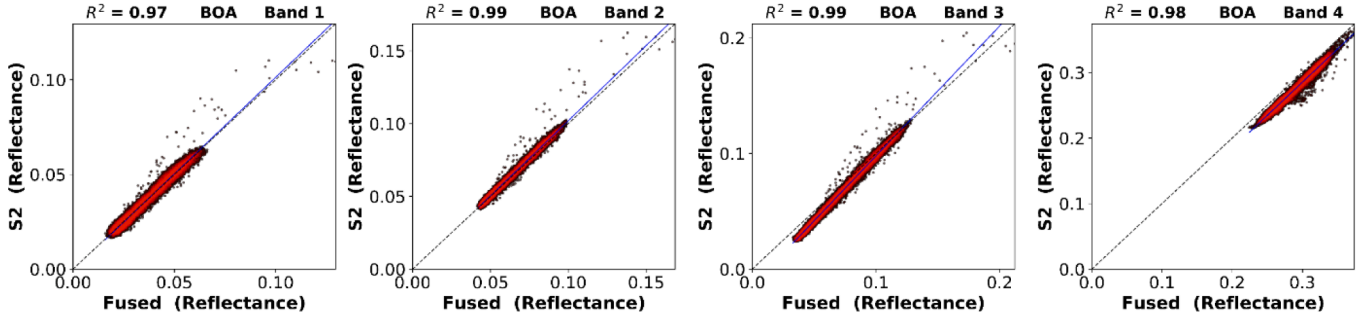

Fig. 4. An example of the correlation between a same day pair of an original S2 image and a fused image (image date 23/7/18) for the field near Birchip, Victoria, Australia. Each scatterplot represents the comparison of a different spectral band, where band 1, 2, 3 and 4 represents the Blue, Green, Red and NIR wavelengths, respectively and the pixels values are in surface reflectance (BOA). The blue line in the figures is the trend line. The dotted line is the 1:1 line. (For interpretation of the references to color in this figure legend, the reader is referred to the web version of this article.)

Table 2
Comparison of the median and mean correlation (R^2) that was found between S2, PS and the fused images of all the images analysed across all sites (2,463 images in each dataset), for each band and all four bands together.

Datasets	Blue (band 1)		Green (band 2)		Red (band 3)		NIR (band 4)		All bands	
	Median	Mean	Median	Mean	Median	Mean	Median	Mean	Median	Mean
PS - S2	0.53	0.46	0.71	0.58	0.75	0.6	0.81	0.75	0.7	0.6
Fused - PS	0.86	0.79	0.9	0.82	0.91	0.84	0.94	0.91	0.9	0.84
Fused - S2	0.9	0.81	0.95	0.88	0.96	0.88	0.96	0.93	0.94	0.88

based LAI maps at the pixel level and at the field level (Fig. 7). Next, remotely-sensed LAI estimations from both S2 and fused images were compared with *in-situ* LAI measurements conducted in the field (Fig. 7).

3.3. LAI estimations

Overall, 57 *in-situ* LAI measurements conducted across 12 wheat fields, half located in Australia and the other half in Israel, were available to evaluate the accuracy of the remotely-sensed LAI estimations. S2-based LAI was found to have an RMSE of 1.60 (R^2 = 0.84), while the RMSE for fused-based LAI estimations ranged from 1.73 to 1.78 depending on the VI considered (R^2 = 0.82–0.84; Table 3). In general, both S2 and fused-based LAI estimations tended to underestimate the *in-situ* LAI values, especially in LAI values larger than 3 (Fig. 8). In comparison with the *in-situ* measurements, S2-based LAI estimations generally had slightly better accuracy compared to VI-based LAI estimations. As optical remote sensing is mainly estimating the Green LAI (Haboudane et al., 2004), the results have been separated into two groups, the *in-situ* measurements conducted when the crops were at the Green LAI stage (Table 3B) and the measurements that were performed during the senescing stage (Table 3C). The peak of the fusion-based LAI was used as the threshold to define these two groups. When analysing the Green LAI separately, the accuracy of the remotely sensed LAI estimations was found to be much higher (Table 3). Overall, remotely-sensed LAI estimations during the Green LAI phase were found to have an RMSE of 1.08 (R^2 = 0.95) for the S2-based LAI, and an RMSE of 1.37–1.4 (R^2 = 0.92–0.94) for the fused-based LAI estimated from the different VIs (Table 3B). S2-based LAI median error for the Green LAI was only −0.38 and the fused-based LAI from best performing VI, i.e., RDVI, had a median error of −0.73 (Table 3B).

Hence, estimating Green LAI using the new method, or with S2-based LAI estimations, was highly correlated to *in-situ* measurement when the crops were still mostly photosynthetically active. However, underestimations of high LAI values (>3) was observed in all studied fields (Fig. 8), probably due to increasing overlap of leaves with higher LAI. One of the main disadvantages of using normalized difference VIs (e.g., NDVI) to remotely estimate LAI is the fact that they tend to saturate asymptotically under conditions of medium-to-high aboveground

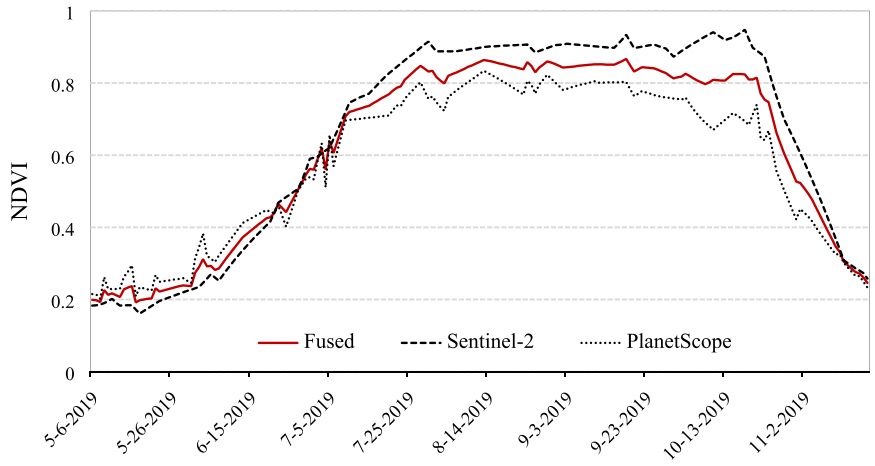

Fig. 5. Six-month time series of Sentinel-2 (black dashed line), PlanetScope (dot line) and the fused images (red line) NDVI calculated from atmospherically corrected bottom of atmosphere (BOA) reflectances. The data represent the daily mean NDVI for a 131-ha wheat field located near Birchip, Victoria, Australia. (For interpretation of the references to color in this figure legend, the reader is referred to the web version of this article.)

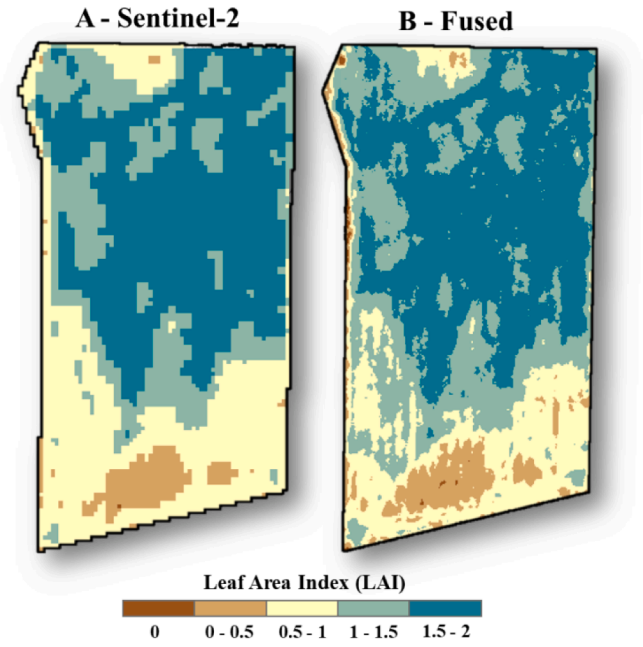

Fig. 6. Comparison between (A) S2-based LAI map (10 m) and (B) S2-PS fusion-based LAI (3 m) map (image date – 7/8/18) of an 88-ha wheat field near Birchip, Victoria, Australia.

biomass density (Gitelson, 2004). To minimise these underestimations, a correction equation was sought for the different VI-based fused dataset and the S2-based LAI. Polynomial order two regression was found as the most suitable to fit the fused-based Green LAI estimates against *in-situ* LAI measurements (Fig. 8 and Table 4), with an R^2 of 0.95 (RMSE of 0.62) for the S2-based LAI, and an R^2 ranging between 0.92 and 0.94 depending on the VI considered (RMSE of 0.67–0.78). Overall, the SR, MTVI2 and RDVI indices showed the best fits.

3.4. Adjustment of S2 LAI to estimate Green LAI in wheat

The equations presented in Table 4 were used to correct, for the different fusion-based LAI and S2-based LAI, the underestimation of the remotely sensed Green LAI estimations (as illustrated in Fig. 9). The performance of the proposed correction method was tested using an independent LAI dataset that was collected in two wheat fields located near Yanco, NSW, Australia. The performance of this method was evaluated for estimating Green LAI with and without the proposed correction.

The results of the Green LAI correction analysis showed that the estimations of the fused-based LAI were improved by up to 47% compared with non-corrected Green LAI estimations (Table 5). The RMSE between the *in-situ* LAI and the fused-based LAI before the correction ranged between 0.53 and 0.87 (among the different indices), while the correction achieved higher accuracy with RMSE ranging between 0.35 and 0.63, as shown in Table 5. Even though the proposed correction aimed to adjust the Green LAI phase of the wheat, the results show that this method also adjusts LAI estimations at the senescing phase. In the conditions tested, the best pre-correction performing indices were for MSAVI, MTVI2 and GNDVI (all < 0.6 RMSE) and the best post-correction performing indices were for GNDVI, Green WDRVI, GDVI, GSR, TVI, OSAVI and NDVI (all < 0.45 RMSE). Overall, the RMSE of Green LAI estimations improved by more than 25% for 10 out of the 13 indices analysed. As for the S2-LAI estimations, in these fields, the S2-LAI underperformed the fused-based LAI estimations having an RMSE of 1.38 ($R^2 = 0.41$). This stems from the fact that the *in-situ* LAI was measured along the edges of these fields. Therefore, the 10 m spatial resolution of S2 suffered from mixed pixels, representing not only the wheat LAI but also the road around the fields, while the 3 m fused LAI images overcame this limitation.

4. Discussion

Monitoring crop performance is essential to guarantee a high quality and profitable yield; however, it has always been a challenge, especially with the large fields that are common to modern agriculture. The large cultivated areas and the frequent monitoring requirement (Waldner et al., 2019), makes remote sensing a valuable tool for farmers and agronomists to achieve maximum yield (Raun et al., 2002).

4.1. The advantages of the proposed fusion approach

CubeSats, such as Planet's PS, are relatively cheap to build and can offer high spatio-temporal imagery at lower costs than traditional satellites. However, CubeSat constellations tend to suffer from cross-sensor inconsistencies in radiometric quality and dissimilarity of their spectral responses among satellites in the constellation, contributing to the noise observed in time-series data acquired from these sensors (Houborg and McCabe, 2016, 2018a). Such inconsistencies limit the accuracy of surface reflectance-based applications such as estimation of vegetation

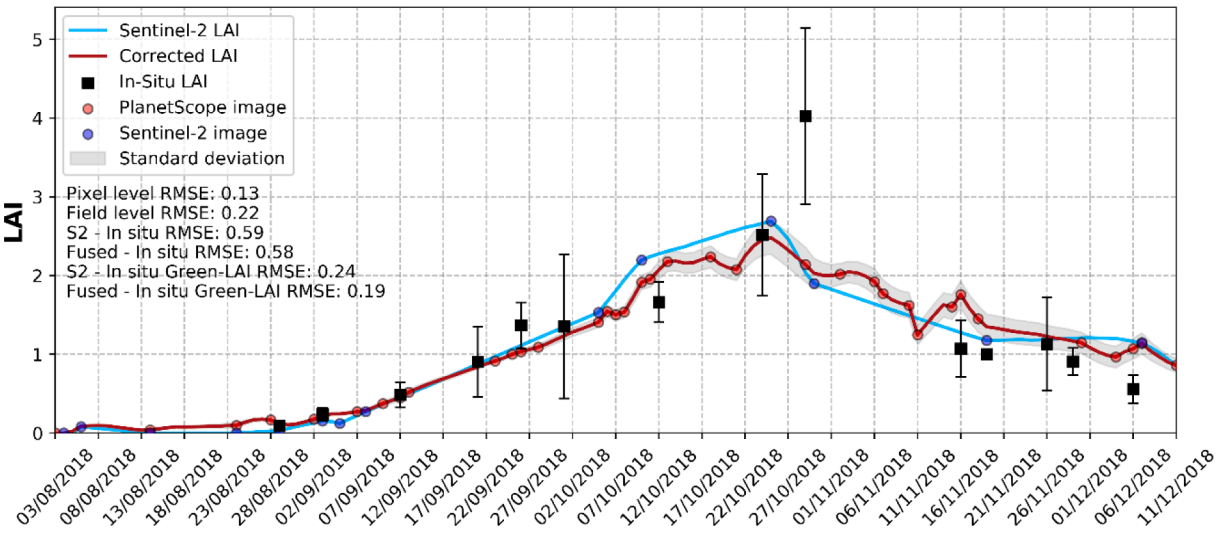

Fig. 7. Comparison of the changes in LAI estimated over the growing season through *in-situ* point measurements (black dots, were the error bars represent the measurements standard deviation), S2 images (blue line) and the fused method (red line) of the 2018 Cora Lynn wheat trial. In this example, the fused-based Renormalized Difference Vegetation Index (RDVI) was used to calculate LAI using a linear regression modal. RMSE is presented (i) between the S2-based LAI to the fused-based LAI estimations at the pixel (Pixel level RMSE') and the field levels (median daily error at the pixel level; 'Field level RMSE'), (ii) between the S2-LAI and *in-situ* LAI measurements ('S2 – *In-situ* RMSE'), (iii) between the Fused images-LAI and *in-situ* LAI measurements ('Fused – *In-situ* RMSE'), (iv) between the S2-LAI and the Green LAI *in-situ* measurements only ('S2 – *In-situ* Green LAI RMSE'), and between the Fused images-LAI and the Green LAI *in-situ* measurements only ('Fused – *In-situ* Green LAI RMSE'). In this example, *in-situ* LAI measurement performed on the 29/10/18 were unusually high, and in any case, much higher than the estimated remotely-sensed LAI. This could be partly due to measurement error (the error bar was also big) combined with the known underestimation of S2-LAI for high LAI values. (For interpretation of the references to color in this figure legend, the reader is referred to the web version of this article.)

indices (Fig. 5), hindering the use of CubeSat satellites to monitor changes on the Earth surface (Sadeh et al., 2019) and for land surface characterization (Houborg and McCabe, 2018a). Fusion of CubeSat imagery with a consistent and reliable dataset, such as S2, can overcome this limitation and eliminate the noise that exists in CubeSat data (Houborg and McCabe, 2018a; Kimm et al., 2020). PS bands have different bandwidths and spectral responses from S2 (Fig. 1). While S2 RGB-NIR bands have a clear spectral separation between the bands, PS's RGB bands overlap each other. Such overlaps can cause contamination of the signals acquired by each band, with radiation belonging to neighbouring bands, limiting the accuracy of different applications such as VI calculations and classification.

The fusion approach proposed in this study helps to resolve the challenges posed by PS spectral responses, producing time-series of images that preserve both the high spatial and temporal resolution of PS and the spectral quality of S2 (as shown in Figs. 3 and 4). In practical terms this means that S2-consistent, surface reflectance RGB-NIR images and crop Green LAI could be generated at a 3 m resolution on a daily basis.

The fusion method proposed here can process a time series from an unlimited number of images to generate a time series of images that covers the whole growing season. This make the method robust and flexible, and the user can theoretically fuse images acquired by a number of sensors. The fleet of Earth observing satellites is increasing every year, offering unprecedented imagery in a range of spectral resolutions acquired across various bands. However, some previous image fusion methods are limited to a maximum of three input bands of a lower resolution at a time (Gašparović and Jogun, 2018). This method is not limited by the number of bands to be fused, so long as the higher spatial-resolution bands covers the spectral range of the lower resolution bands. In order to reduce sampling gaps between images sourced from one dataset such as S2, the method can also use Landsat images for example, to increase the temporal resolution of these coarse images. In the same way, if a new CubeSat constellation that can provide data complimentary to PS becomes operational, it can be integrated as an additional high spatio-temporal imagery in the fusion process.

The potential of spaceborne remote sensing to provide relevant information by monitoring crop performance has long been recognized. However, despite the technological and methodological progress over the past decades, remotely sensed data are still not as broadly and operationally used by farmers as they should be. This could be because of the cost of images with both high temporal (<5 days) and spatial resolutions (<5 m) (e.g. DigitalGlobe's WorldView-2 and 3), which limit the profitability of the farm. Or it could be that agronomists and farmers do not have the knowledge and skills required to process and analyse the satellite data. This study has addressed the issue of availability for affordable high spatio-temporal data for crop monitoring at a field and sub-field scale. In addition, such new datasets can be used for precision agriculture applications, which until now couldn't be implemented owing to the temporal or spatial limitation of the existing publicly available sources of satellite data.

Near real-time estimation of Green LAI can provide farmers with the tool to monitor the crop health and growth status, which may support farm management actions such as irrigation and fertilization (Pasqualotto et al., 2019). However, waiting for a cloud free image from the publicly available satellite imagery (e.g. S2 and Landsat), often results in an image that is too late to act in the field or will result in an incorrect interpretation (Khan et al., 2018). For example, the peak of the crop LAI, which has been found to be as an important parameter to provide early estimates of grain yield (Waldner et al., 2019), can be easily missed by the 16 and 5 day revisit times of Landsat (Jin et al., 2017) and S2 (Clevers et al., 2017), respectively. Consequently, methods developed for yield estimation based on the peak of VIs (e.g. Franch et al., 2015) or LAI (e.g. Lobell et al., 2015) are not able to provide accurate yield estimates, or to target small farm holders fields. The proposed method allows time-series gaps due to clouds to be filled and improves the probability of identifying the peak LAI. However, it still faces some limitations in near real-time monitoring on cloudy days.

4.2. Estimating wheat Green LAI

Similar to previous studies (e.g. Dhakar et al., 2019; Djamai and Fernandes, 2018; Djamai et al., 2019; Pasqualotto et al., 2019), this study found S2 LAI products (created using the Biophysical Processor

Table 3
Performance of remotely-sensed LAI estimations for both S2-based and the fused-based LAI compared to the *in-situ* LAI measurements. The best performing index from the VIs-based fusion is coloured in red. Indices of the S2-based LAI estimations are coloured in green when they performed better than the fused data. Table A presents the results for all of the LAI measurements conducted in the field (n = 57), table B refers only to *in-situ* measurements conducted when the crops were at the Green LAI stage (n = 25) and table C presents the results only for LAI measurements conducted in the field during the senescing stage of the crops (n = 32). Overall, the best accuracy was achieved during the Green LAI stage (table B).

(A) **All samples (n = 57)**

	S2 LAI	EVI2	GCVI	GNDVI	Green-WDRVI	GSR	MSAVI	MTVI2	NDVI	OSAVI	RDVI	TVI	WDRVI	SR
RMSE	1.60	1.77	1.77	1.78	1.77	1.77	1.77	1.74	1.77	1.77	1.77	1.77	1.76	1.73
R^2	0.84	0.83	0.84	0.83	0.83	0.84	0.82	0.83	0.82	0.82	0.83	0.83	0.83	0.84
Mean error	-1.08	-1.24	-1.26	-1.26	-1.26	-1.26	-1.24	-1.22	-1.24	-1.24	-1.24	-1.25	-1.24	-1.23
Median error	-0.55	-0.85	-0.93	-0.91	-0.93	-0.93	-0.83	-0.86	-0.84	-0.84	-0.91	-0.84	-0.88	-0.88
Mean accuracy %	79.52	76.13	75.02	75.26	75.11	75.03	76.25	76.88	76.18	76.18	77.11	76.16	75.98	75.96
Median accuracy %	76.62	74.41	73.24	73.64	73.38	73.27	74.46	75.37	74.39	74.39	74.20	75.45	73.84	72.41

(B) **Green LAI only (n = 25)**

	S2 LAI	EVI2	GCVI	GNDVI	Green-WDRVI	GSR	MSAVI	MTVI2	NDVI	OSAVI	RDVI	TVI	WDRVI	SR
RMSE	1.08	1.39	1.39	1.38	1.39	1.39	1.38	1.37	1.39	1.39	1.38	1.38	1.40	1.37
R^2	0.95	0.93	0.93	0.92	0.92	0.93	0.93	0.94	0.93	0.93	0.94	0.93	0.93	0.94
Mean error	-0.68	-0.95	-0.97	-0.95	-0.96	-0.97	-0.94	-0.93	-0.94	-0.94	-0.96	-0.94	-0.96	-0.95
Median error	-0.38	-0.83	-0.87	-0.80	-0.84	-0.87	-0.81	-0.74	-0.82	-0.82	-0.73	-0.82	-0.85	-0.87
Mean accuracy %	90.85	84.84	83.74	84.12	83.86	83.76	85.08	85.58	84.92	84.92	86.49	85.81	84.60	84.65
Median accuracy %	86.95	79.73	76.34	78.33	76.69	76.34	80.57	80.44	80.15	80.15	81.37	80.47	79.63	79.33

(C) **LAI of senescing canopy (n = 32)**

	S2 LAI	EVI2	GCVI	GNDVI	Green-WDRVI	GSR	MSAVI	MTVI2	NDVI	OSAVI	RDVI	TVI	WDRVI	SR
RMSE	1.90	2.02	2.01	2.03	2.02	2.01	2.02	1.99	2.02	2.02	2.02	2.02	2.00	1.97
R^2	0.83	0.79	0.81	0.80	0.81	0.81	0.79	0.79	0.79	0.79	0.79	0.80	0.80	0.80
Mean error	-1.41	-1.51	-1.51	-1.52	-1.52	-1.51	-1.51	-1.49	-1.51	-1.51	-1.51	-1.52	-1.50	-1.48
Median error	-1.08	-1.16	-1.23	-1.25	-1.24	-1.23	-1.16	-1.11	-1.16	-1.16	-1.14	-1.16	-1.16	-1.13
Mean accuracy %	70.66	69.32	68.21	68.33	68.27	68.22	69.35	70.09	69.35	69.35	69.78	68.63	69.24	69.18
Median accuracy %	62.58	62.73	58.58	59.80	59.07	58.58	60.83	61.06	62.01	62.01	59.78	61.11	61.74	59.95

within ESA's SNAP software (Weiss and Baret, 2016)) are capable of estimating wheat Green LAI (R^2 = 0.95 and 1.08 RMSE). However, the S2-LAI product was found to be less suitable for estimating wheat senescence-LAI (R^2 = 0.83 and 1.9 RMSE). One of the strengths of this new method for estimating LAI is the fact that it combines both methods, i.e., the physically-based retrieval method (e.g. RTM) and the empirical approach (e.g. using VIs), to convert surface reflectance data into LAI estimates. First, the method uses the RTM-based S2-LAI product as a benchmark and then uses the fused VI image pixel values within the defined region of interest, as an automatic "field-based" calibration to convert the fused VIs into S2-like LAI estimates, through a series of linear regression models. These regressions, which are automatically generated for each day in the time-series, are uniquely fitted to the area of interest (e.g. the analysed field). This approach enables the method to be more robust and valid across different soil types, crop types and varieties, farm managements and environmental conditions.

In this study, 13 different VIs were tested (Table 1), having been indicated in the literature to be highly correlated with LAI, and evaluated their performance to estimate LAI in the new fusion method. It was found that overall this new method is not sensitive to a specific VI, with the fused Green LAI estimates from the various indices ranging from RMSE 1.37–1.4 (R^2 = 0.92–0.94). The MTVI2, SR and the RDVI were found to be the best preforming VIs in this study. However, all of these VI fuse-based estimates slightly underperformed the accuracy of S2 Green LAI estimations (Table 4) while also providing daily estimates at 3 m resolution.

The S2-LAI product has a few limitations. As noted by previous studies, similar to other remotely sensed LAI estimation (e.g. Djamai et al., 2019; Houborg et al., 2016), S2-based Green LAI estimates also tend to underestimate high Green LAI values (LAI > ~3) (Dhakar et al., et al., 2019; Djamai et al., 2019; Herrmann et al., 2011; Pasqualotto et al., 2019; Verrelst et al., 2015). These underestimations are probably produced by the asymptotically saturation of the surface reflectance data caused by the high biomass density (Gitelson, 2004). These underestimations become even more significant from LAI = 6 and higher (as shown in Fig. 8), which causes the uncertainties in estimating high LAI values (LAI > 6) using SNAP's Biophysical Processor, as reported by Weiss and Baret (2016). The analysis of the new fused LAI time series showed similar underestimations as the S2-LAI, which is not surprising considering the fact that the fused-LAI was created using S2-LAI data.

Similar to other LAI products such as MODIS LAI (Myneni and Park, 2015) or Visible Infrared Imaging Radiometer Suite (VIIRS) LAI products (Knyazikhin and Myneni, 2018), the S2-LAI product uses a generic method to estimate LAI for any type of vegetation (Weiss and Baret, 2016). Therefore, in order to have a better match for a specific crop type, a correction should be applied to calibrate the data (Weiss and Baret, 2016). This study has developed regression models (Table 4) to adjust both the S2-based LAI and the fused-LAI estimates to provide more accurate wheat LAI estimates. The performance of the proposed correction, which was tested using an independent wheat LAI dataset measured in NSW, Australia, showed a clear improvement in the accuracy of the method to estimate wheat Green LAI. In 10 out of the 13

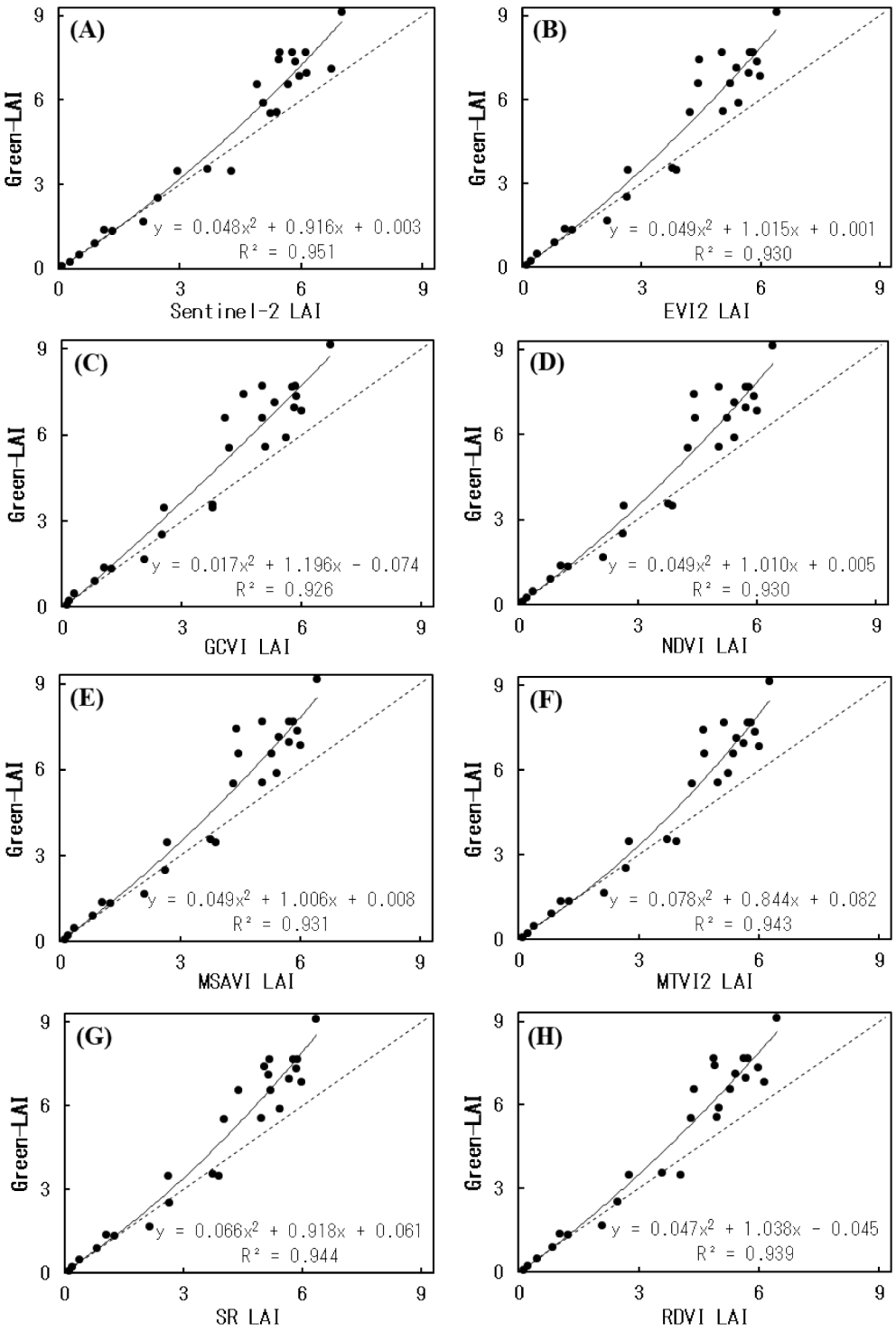

Fig. 8. Example of *in-situ* vs. remotely sensed Green LAI: (A) Sentinel-2 based LAI (B) Enhanced Vegetation Index 2 (EVI2), (C) Green Chlorophyll Vegetation Index (GCVI), (D) Normalized Difference Vegetation Index (NDVI), (E) Modified Soil-Adjusted Vegetation Index (MSAVI), (F) Modified Triangular Vegetation Index 2 (MTVI2), (G) Simple Ratio (SR), (H) Renormalized Difference Vegetation Index (RDVI). In all plots, solid line is best-fit function, dashed line is the one-to-one line. Statistics relative to these fits are presented in Table 4.

indices tested, the RMSE of Green LAI estimates improved by more than 25%, while four improved by more than 39% (Green WDRVI improved in 47%) in comparison with non-corrected Green LAI estimations (Table 5), with RMSE ranging between 0.35 and 0.63. The S2-LAI data was also tested, however the comparison between the pre-correction and the post-correction Green LAI estimates showed that S2-LAI underperformed the fused-based LAI estimates with 1.38 RMSE ($R^2 = 0.41$). The reason that the S2-LAI data was not able to reproduce the accuracy achieved by the fused data to estimate the Green LAI is due to the fact that the *in-situ* LAI in these fields was measured along the fields' boundaries, and therefore, the S2 data suffered from mixed pixels that lowered the Green LAI estimates. The mixed pixel effect has long been recognised as a main drawback to monitor crop performance and characterization from space, especially when using low and medium spatial resolution data such as the imagery acquired by MODIS and Landsat (Gao et al., 2012, 2006; Jain et al., 2016; Khan et al., 2018; Li et al., 2019). While LAI information driven from low to medium resolution satellite images may be lost for certain surface types that appear only at smaller spatial scales (Gao et al., 2012), the 3 m fused LAI data presented in this study overcome these limitations.

Despite the fact that the proposed correction aimed to adjust the Green LAI phase of the wheat, the results shows that the accuracy of the

Table 4
Best-fit functions of the relationships between Green LAI and VI's obtained using a cross-validation procedure for wheat, when x = VI, y = Green LAI, and the RMSE is the root mean squared error of the Green LAI estimation. Fits were performed for data of all the studied trials and are presented in Fig. 8.

VI	Equation	R^2	RMSE
Sentinel-2 LAI	$y = 0.0482x^2 + 0.9161x + 0.0026$	0.95	0.62
SR	$y = 0.0658x^2 + 0.9179x + 0.0614$	0.94	0.67
MTVI2	$y = 0.0784x^2 + 0.8443x + 0.0823$	0.94	0.68
RDVI	$y = 0.0475x^2 + 1.0382x - 0.0452$	0.94	0.70
WDRVI	$y = 0.0502x^2 + 1.0139x + 0.0005$	0.93	0.74
MSAVI	$y = 0.0493x^2 + 1.006x + 0.0085$	0.93	0.74
TVI	$y = 0.0464x^2 + 1.0279x - 0.0131$	0.93	0.75
OSAVI	$y = 0.0492x^2 + 1.0102x + 0.0052$	0.93	0.75
NDVI	$y = 0.0492x^2 + 1.0102x + 0.0051$	0.93	0.75
EVI2	$y = 0.0489x^2 + 1.015x + 0.0012$	0.93	0.75
GSR	$y = 0.0171x^2 + 1.196x - 0.0743$	0.93	0.77
GCVI	$y = 0.0171x^2 + 1.1961x - 0.074$	0.93	0.77
Green WDRVI	$y = 0.0164x^2 + 1.1967x - 0.0726$	0.92	0.78
GNDVI	$y = 0.0183x^2 + 1.1786x - 0.0599$	0.92	0.78

LAI estimations of the senescing phase has also improved after applying the correction. Future study should attempt to develop an adjustment method that will target the crop's senescing phase only. As demonstrated in Fig. 6, the new high-resolution dataset was able to better describe the spatial patterns of the crops and to identify vegetation with less active growth within the sub-field scale. Moreover, the new high spatio-temporal LAI estimates can be potentially used to monitor crops grown on small holder (<2 ha) farms in developing countries (Jain et al., 2016). Nevertheless, it is expected that the regression models proposed here to correct S2 Green LAI estimations will exceed those of the non-corrected wheat Green LAI estimates, when overcoming the mixed pixel effect. However, this should be further tested in future studies.

4.3. Limitations and prospects

Even with the promising results presented here, there are some limitations that should be noted. The fused daily 3 m LAI data was evaluated across two countries in four different geographic locations, over 12 wheat fields with diverse farm management practices, soil types, climates and varieties. However, the correction method presented in this study to adjust the S2 and fused Green LAI was tested in one geo-location only. Therefore, future studies should explore the performance of the proposed correction over a larger number of fields and environments.

While some previous studies have suggested that red-edge based VIs may help to mitigate the saturation problem encountered when estimating high LAI values using traditional VIs based on visible reflectance, such as NDVI (Dong et al., 2019; Nguy-Robertson et al., 2012). Nguy-Robertson et al., (2014) have shown that this is not universally true.

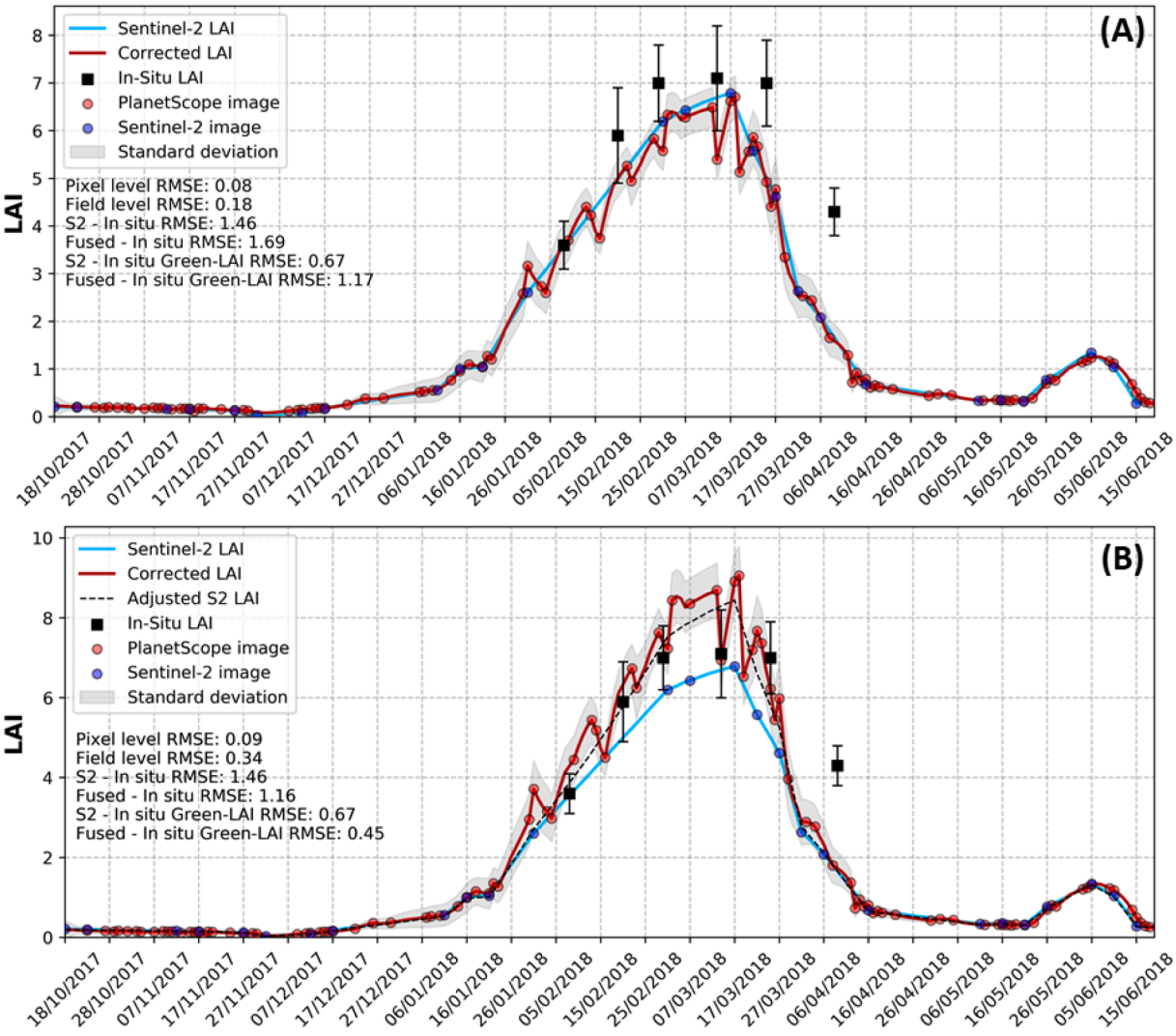

Fig. 9. Change over time in LAI for pre- (A) and post- (B) corrected LAI values in a wheat field in Saad in 2018. See caption of Fig. 7 for details of the legend. (The field which presented in this figure was not used as part of the independent LAI dataset, it is used here as it illustrates best the adjustment concept).

Table 5
Performance of remotely-sensed Green LAI estimates compared to *in-situ* LAI measurement for pre and post Green LAI correction. This table presents the RMSE between the *in-situ* Green LAI measurements of an independent dataset (fields of Yanco) and the Green LAI estimated from the fused data and S2 images. Best performing index are coloured in red.

Green LAI	*S2 LAI*	*EVI2*	*GCVI*	*GNDVI*	*Green-WDRVI*	*GSR*	*MSAVI*	*MTVI2*	*NDVI*	*OSAVI*	*RDVI*	*TVI*	*WDRVI*	*SR*
RMSE (pre-correction)	1.38	0.75	0.76	0.58	0.76	0.76	**0.53**	0.56	0.65	0.65	0.68	0.61	0.87	0.84
RMSE (post-correction)	1.38	0.50	0.43	**0.35**	0.40	0.43	0.45	0.57	0.44	0.44	0.54	0.44	0.62	0.63
Improvement in RMSE	0%	34%	43%	39%	**47%**	43%	14%	-1%	31%	32%	21%	28%	29%	25%
R^2 *(pre-correction)*	0.412	0.767	**0.921**	0.584	0.761	**0.921**	0.272	0.024	0.439	0.481	0.519	0.365	0.906	0.748
R^2 *(post-correction)*	0.411	0.764	**0.920**	0.584	0.760	**0.920**	0.270	0.024	0.433	0.475	0.527	0.359	0.898	0.746

Moreover, current PlanetScope imagery does not provide red-edge data and so was not applied in this study.

Even though it is one of the cheapest commercial high-resolution image products currently available in the market, Planet's PS images are not free like S2. Farmers and others, who may want to use such high spatio-temporal LAI and VIs data, should consider the cost effectiveness of this data. It is expected that high-performing farmers will find it very beneficial while individual farmers in developing countries may find the costs too high. As more CubeSat constellations come on line in coming years, prices of their imagery will likely be reduced.

The uncertainty of the PlanetScope data in terms of its geo-location accuracy has been reported as less than 10 m RMSE (Planet Team, 2018). This uncertainty may affect the utility of the PlanetScope data when carrying out detailed time-series analyses (Houborg and McCabe, 2018b). Implementing a co-registration practice to reduce the cross-scene co-registration error, similar to the co-registration technique proposed by Houborg and McCabe (2018b), is likely to increase the spatial correlation between consecutive scenes.

This study used a simple linear interpolation to fill data gaps between the cloud free images for both PS and S2 images to create evenly spaced time series. Despite the simplicity of this approach, previous studies showed that linear interpolation is an effective way to interpolate between periods with valid data to assign values to the periods of missing satellite observations with considerable accuracy (Maynard et al., 2016; Pan et al., 2015; Sakamoto et al., 2010; Zhu et al., 2011). Importantly, this study implemented a fusion method to monitor field crops, which commonly do not change over a single day. This method can therefore be used for other disciplines that also have a slow temporal evolution, such as forestry, land cover classification (Gašparović et al., 2018), geomorphological and environmental studies, or to monitor urban development over time. Nevertheless, the utility of its implementation for monitoring rapidly changing environments or phenomena such as flash floods or fires, should be further investigated and evaluated compared to change detection techniques (e.g. Sadeh et al., 2019).

As a prospect for future improvements and research directions, it is suggested that future studies should test the proposed fusion method over other crops types, explore the possibility of adding more sensors in the fusion process (e.g. Landsat) and examine the suitability of this fusion method to fuse other sensor data (other than S2 and PS). Although this study attempted to generate high resolution LAI, this method can potentially be useful to produce high spatio-temporal time series of Fraction of Absorbed Photosynthetically Active Radiation (FAPAR), Fraction of vegetation cover (FCOVER), Chlorophyll content in the leaf (Cab) and Canopy Water Content (CWC). Furthermore, future studies should explore the suitability of the proposed fusion method for improving the spatial and temporal data obtained from sensors operated in the shortwave infrared (SWIR) and the thermal wavelengths, such as those on-board Landsat and S2.

5. Conclusion

With the increasing number of CubeSat constellations expected to become operational in the coming years, a new era of Earth observing satellite-based applications has begun. This paper presents the first study to fuse time series imagery sourced from Sentinel-2 (S2) and Planets' PlanetScope (PS) CubeSat constellation. The fusion method proposed in this study enabled S2-consistent, cloud free, surface reflectance RGB-NIR images and crop Green LAI to be generated at a 3 m resolution. Overall, the results from the study demonstrated that the new fused time-series data combined the spatial, temporal and spectral advantages of both sensors, allowing wheat Green LAI to be monitored on a daily basis with an RMSE of 1.37 and R^2 of 0.94 in wheat.

Furthermore, this study proposed a correction method to compensate the underestimations in high LAI values (greater than 3) between the remotely sensed LAI estimations and the *in-situ* measurements. With the implementation of the correction method, the accuracy of the Green LAI estimations improved by up to 47% (RMSE = 0.35–0.63).

Although tested to fuse S2 and PS data for LAI estimations, this new time series fusion method can be used to fuse other sources of imagery with different spectral, spatial and temporal resolutions. Furthermore, it may be used to estimate indices or parameters other than LAI. The proposed method is not limited to a specific number of bands, wavelengths or images, and can integrate numerous sources of imagery. This new time series fusion method can be used for continuous daily high-resolution monitoring of crops over large scales, and can potentially be used for a range of new precision agriculture applications. Such time-series are critical for crop health and growth status monitoring, and will improve the effectiveness of farming practices such as water management and fertilization, as well as improve yield forecasts.

CRediT authorship contribution statement

Yuval Sadeh: Conceptualization, Methodology, Software, Validation, Formal analysis, Resources, Writing - original draft, Visualization. **Xuan Zhu:** Supervision, Writing - review & editing. **David Dunkerley:** Supervision, Writing - review & editing. **Jeffrey P. Walker:** Supervision, Writing - review & editing. **Yuxi Zhang:** Investigation, Formal analysis, Writing - review & editing. **Offer Rozenstein:** Investigation, Formal analysis, Writing - review & editing. **V.S. Manivasagam:** Investigation, Formal analysis, Writing - review & editing. **Karine Chenu:** Methodology, Supervision, Writing - review & editing.

Declaration of Competing Interest

The authors declare that they have no known competing financial interests or personal relationships that could have appeared to influence the work reported in this paper.

Acknowledgments

The authors would like to thank Tim McClelland (Partner A.W. McClelland & Co, Birchip VIC 3483, Australia) and Wayne Tymensen (farmer at Eleven Mile Road, Cora Lynn, VIC 3814, Australia) for providing the access to their farms to measure LAI data. Planet Labs, Inc. for providing us with the PlanetScope imageries used in this study. Ben Knight from the School of Earth, Atmosphere and Environment at Monash University, for his contribution over the field work conducted at Birchip and his assistance with the coding, Australia. Xiaoling Wu, Xiaoji Shen, and Nithyapriya Boopathi from the Department of Civil Engineering at Monash University, for their assistance in the wheat sample collection at Cora Lynn farm, Australia. Field measurements in Israel were supported by the Ministry of Science, Technology, and Space, Israel, under grant number 3-14559. This work was supported by the Co-Funded Monash Graduate Scholarship awarded to Y. Sadeh by Monash University.

References

Australian Bureau of Meteorology. 2020. "Australian Bureau of Meteorology." Bureau of Meteorology, Accessed 12/8/2020. http://www.bom.gov.au/climate/data/?ref=ftr.

Azzari, G., Jain, M., Lobell, D.B., 2017. Towards fine resolution global maps of crop yields: testing multiple methods and satellites in three countries. Remote Sensing Environ.

Bøgh, E., Thorsen, M., Butts, M., Hansen, S., Christiansen, J., Abrahamsen, P., et al., 2004. Incorporating remote sensing data in physically based distributed agro-hydrological modelling. J. Hydrol. 287 (1–4), 279–299.

Bsaibes, A., Courault, D., Baret, F., Weiss, M., Olioso, A., Jacob, F., et al., 2009. Albedo and LAI estimates from FORMOSAT-2 data for crop monitoring. Remote Sens. Environ. 113 (4), 716–729.

Chen, J.M., Pavlic, G., Brown, L., Cihlar, J., Leblanc, S.G., White, H.P., et al., 2002. Derivation and validation of Canada-wide coarse-resolution leaf area index maps using high-resolution satellite imagery and ground measurements. Remote Sens. Environ. 80 (1), 165–184.

Clevers, J.G.P.W., 1991. Application of the WDVI in estimating LAI at the generative stage of barley. ISPRS J. Photogramm. Remote Sens. 46 (1), 37–47.

Clevers, J.G.P.W., Kooistra, L., van den Brande, M.M.M., 2017. Using Sentinel-2 data for retrieving LAI and leaf and canopy chlorophyll content of a potato crop. Remote Sensing 9 (5).

Daughtry, C., Gallo, K., Goward, S., Prince, S., Kustas, W., 1992. Spectral estimates of absorbed radiation and phytomass production in corn and soybean canopies. Remote Sens. Environ. 39 (2), 141–152.

Delegido, J., Verrelst, J., Rivera, J.P., Ruiz-Verdú, A., Moreno, J., 2015. Brown and green LAI mapping through spectral indices. Int. J. Appl. Earth Obs. Geoinf. 35, 350–358.

Dhakar, R., Sehgal, V.K., Chakraborty, D., Sahoo, R.N., Mukherjee, J., 2019. Field scale wheat LAI retrieval from multispectral Sentinel 2A-MSI and LandSat 8-OLI imagery: effect of atmospheric correction, image resolutions and inversion techniques. Geocarto Int. 1–21.

Djamai, N., Fernandes, R., 2018. Comparison of SNAP-derived Sentinel-2A L2A product to ESA product over Europe. Remote Sensing 10 (6), 926.

Djamai, N., Fernandes, R., Weiss, M., McNairn, H., Goïta, K., 2019. Validation of the Sentinel Simplified Level 2 Product Prototype Processor (SL2P) for mapping cropland biophysical variables using Sentinel-2/MSI and Landsat-8/OLI data. Remote Sens. Environ. 225, 416–430.

Dong, T., Liu, J., Shang, J., Qian, B., Ma, B., Kovacs, J.M., et al., 2019. Assessment of red-edge vegetation indices for crop leaf area index estimation. Remote Sens. Environ. 222, 133–143.

Drusch, M., Del Bello, U., Carlier, S., Colin, O., Fernandez, V., Gascon, F., et al., 2012. Sentinel-2: ESA's optical high-resolution mission for GMES operational services. Remote Sens. Environ. 120, 25–36.

El Hajj, M., Baghdadi, N., Cheviron, B., Belaud, G., Zribi, M., 2016. Integration of remote sensing derived parameters in crop models: application to the PILOTE model for hay production. Agric. Water Manag. 176, 67–79.

Fang, H., Baret, F., Plummer, S., Schaepman-Strub, G., 2019. An overview of global leaf area index (LAI): methods, products, validation, and applications. Rev. Geophys. 57 (3), 739–799.

Franch, B., Vermote, E., Roger, J.-C., Murphy, E., Becker-Reshef, I., Justice, C., et al., 2017. A 30+ Year AVHRR land surface reflectance climate data record and its application to wheat yield monitoring. Remote Sensing 9 (3).

Franch, B., Vermote, E.F., Becker-Reshef, I., Claverie, M., Huang, J., Zhang, J., et al., 2015. Improving the timeliness of winter wheat production forecast in the United States of America, Ukraine and China using MODIS data and NCAR Growing Degree Day information. Remote Sens. Environ. 161, 131–148.

Gao, F., Anderson, M.C., Kustas, W.P., Wang, Y., 2012. Simple method for retrieving leaf area index from Landsat using MODIS leaf area index products as reference. J. Appl. Remote Sens. 6 (1), 063554.

Gao, F., Masek, J., Schwaller, M., Hall, F., 2006. On the blending of the Landsat and MODIS surface reflectance: Predicting daily Landsat surface reflectance. IEEE Trans. Geosci. Remote Sens. 44 (8), 2207–2218.

Gašparović, M., Jogun, T., 2018. The effect of fusing Sentinel-2 bands on land-cover classification. Int. J. Remote Sens. 39 (3), 822–841.

Gašparović, M., Medak, D., Pilaš, I., Jurjević, L., Balenović, I., 2018. Fusion of Sentinel-2 and PlanetScope Imagery for Vegetation Detection and Monitorin. In: Volumes ISPRS TC I Mid-term Symposium Innovative Sensing-From Sensors to Methods and Applications.

Gitelson, A., Merzlyak, M.N., 1994. Spectral reflectance changes associated with autumn senescence of Aesculus hippocastanum L. and Acer platanoides L. leaves. Spectral features and relation to chlorophyll estimation. J. Plant Physiol. 143 (3), 286–292.

Gitelson, A.A., 2004. Wide dynamic range vegetation index for remote quantification of biophysical characteristics of vegetation. J. Plant Physiol. 161 (2), 165–173.

Gitelson, A.A., Viña, A., Arkebauer, T.J., Rundquist, D.C., Keydan, G., Leavitt, B., 2003. Remote estimation of leaf area index and green leaf biomass in maize canopies. Geophys. Res. Lett. 30 (5).

Gitelson, A.A., Vina, A., Ciganda, V., Rundquist, D.C., Arkebauer, T.J., 2005. Remote estimation of canopy chlorophyll content in crops. Geophys. Res. Lett. 32 (8).

Haas, R., Deering, D., Rouse Jr, J., Schell, J., 1975. Monitoring vegetation conditions from LANDSAT for use in range management. In: NASA Earth Resources Survey Symposium. NASA. Lyndon B. Johnson Space Center, United States, pp. 43–52.

Haboudane, D., Miller, J.R., Pattey, E., Zarco-Tejada, P.J., Strachan, I.B., 2004. Hyperspectral vegetation indices and novel algorithms for predicting green LAI of crop canopies: modeling and validation in the context of precision agriculture. Remote Sens. Environ. 90 (3), 337–352.

Herrmann, I., Pimstein, A., Karnieli, A., Cohen, Y., Alchanatis, V., Bonfil, D.J., 2011. LAI assessment of wheat and potato crops by VENμS and Sentinel-2 bands. Remote Sens. Environ. 115 (8), 2141–2151.

Houborg, R., McCabe, M., 2016. High-resolution NDVI from Planet's constellation of Earth observing nano-satellites: a new data source for precision agriculture. Remote Sensing 8 (9).

Houborg, R., McCabe, M., 2018a. Daily retrieval of NDVI and LAI at 3 m resolution via the fusion of CubeSat, Landsat, and MODIS Data. Remote Sensing 10 (6), 890.

Houborg, R., McCabe, M.F., 2018b. A Cubesat Enabled Spatio-Temporal Enhancement Method (CESTEM) utilizing Planet, Landsat and MODIS Data. Remote Sens. Environ. 209, 211–226.

Houborg, R., McCabe, M.F., 2018c. A hybrid training approach for leaf area index estimation via Cubist and random forests machine-learning. ISPRS J. Photogramm. Remote Sens. 135, 173–188.

Houborg, R., McCabe, M.F., Gao, F., 2016. A spatio-temporal enhancement method for medium resolution LAI (STEM-LAI). Int. J. Appl. Earth Obs. Geoinf. 47, 15–29.

Huang, J., Ma, H., Su, W., Zhang, X., Huang, Y., Fan, J., et al., 2015. Jointly assimilating MODIS LAI and et products into the SWAP model for winter wheat yield estimation. IEEE J. Sel. Top. Appl. Earth Obs. Remote Sens. 8 (8), 4060–4071.

Ines, A.V., Das, N.N., Hansen, J.W., Njoku, E.G., 2013. Assimilation of remotely sensed soil moisture and vegetation with a crop simulation model for maize yield prediction. Remote Sens. Environ. 138, 149–164.

Israel Meteorological Service, 2020. https://ims.gov.il/en/climateAtlas (accessed 18.08.2020).

Jain, M., Srivastava, A., Balwinder, S., Joon, R., McDonald, A., Royal, K., et al., 2016. Mapping smallholder wheat yields and sowing dates using micro-satellite data. Remote Sensing 8 (10), 860–878.

Jiang, Z., Huete, A.R., Didan, K., Miura, T., 2008. Development of a two-band enhanced vegetation index without a blue band. Remote Sens. Environ. 112 (10), 3833–3845.

Jin, Z., Azzari, G., Lobell, D.B., 2017. Improving the accuracy of satellite-based high-resolution yield estimation: a test of multiple scalable approaches. Agric. For. Meteorol. 247, 207–220.

Jordan, C.F., 1969. Derivation of leaf-area index from quality of light on the forest floor. Ecology 50 (4), 663–666.

Khan, A., Hansen, M.C., Potapov, P.V., Adusei, B., Pickens, A., Krylov, A., et al., 2018. Evaluating landsat and rapideye data for winter wheat mapping and area estimation in punjab, pakistan. Remote Sensing 10 (4), 489.

Kimm, H., Guan, K., Jiang, C., Peng, B., Gentry, L.F., Wilkin, S.C., et al., 2020. Deriving high-spatiotemporal-resolution leaf area index for agroecosystems in the US Corn Belt using Planet Labs CubeSat and STAIR fusion data. Remote Sens. Environ. 239, 111615.

Knyazikhin, Y., Myneni, R., 2018. VIIRS Leaf Area Index (LAI) and Fraction of Photosynthetically Active Radiation Absorbed by Vegetation (FPAR) User Guide.

Leach, N., Coops, N.C., Obrknezev, N., 2019. Normalization method for multi-sensor high spatial and temporal resolution satellite imagery with radiometric inconsistencies. Comput. Electron. Agric. 164, 104893.

LI-COR, I., 1992. LAI-2000 Plant Canopy Analyzer. In: Operating Manual.

Li, W., Jiang, J., Guo, T., Zhou, M., Tang, Y., Wang, Y., et al., 2019. Generating red-edge images at 3 M spatial resolution by fusing Sentinel-2 and planet satellite products. Remote Sensing 11 (12), 1422.

Liu, W., Huang, J., Wei, C., Wang, X., Mansaray, L.R., Han, J., et al., 2018. Mapping water-logging damage on winter wheat at parcel level using high spatial resolution satellite data. ISPRS J. Photogramm. Remote Sens. 142, 243–256.

Lobell, D.B., Thau, D., Seifert, C., Engle, E., Little, B., 2015. A scalable satellite-based crop yield mapper. Remote Sens. Environ. 164, 324–333.

Louis, J., Debaecker, V., Pflug, B., Main-Knorn, M., Bieniarz, J., Mueller-Wilm, U., et al., 2016. Sentinel-2 SEN2COR: L2A processor for users. In: Proceedings of the Living Planet Symposium, Prague, Czech Republic, pp. 9–13.

Luo, Y., Guan, K., Peng, J., 2018. STAIR: A generic and fully-automated method to fuse multiple sources of optical satellite data to generate a high-resolution, daily and cloud-/gap-free surface reflectance product. Remote Sens. Environ. 214, 87–99.

Maynard, J.J., Karl, J.W., Browning, D.M., 2016. Effect of spatial image support in detecting long-term vegetation change from satellite time-series. Landscape Ecol. 31 (9), 2045–2062.
Myneni, R., Park, Y., 2015. MODIS collection 6 (C6) LAI/FPAR product user's guide. In: Feb.
Nguy-Robertson, A., Gitelson, A., Peng, Y., Viña, A., Arkebauer, T., Rundquist, D., 2012. Green leaf area index estimation in maize and soybean: combining vegetation indices to achieve maximal sensitivity. Agron. J. 104 (5), 1336–1347.
Nguy-Robertson, A.L., Peng, Y., Gitelson, A.A., Arkebauer, T.J., Pimstein, A., Herrmann, I., et al., 2014. Estimating green LAI in four crops: potential of determining optimal spectral bands for a universal algorithm. Agric. For. Meteorol. 192, 140–148.
Pan, Z., Huang, J., Zhou, Q., Wang, L., Cheng, Y., Zhang, H., et al., 2015. Mapping crop phenology using NDVI time-series derived from HJ-1 A/B data. Int. J. Appl. Earth Obs. Geoinf. 34, 188–197.
Pasqualotto, N., Delegido, J., Van Wittenberghe, S., Rinaldi, M., Moreno, J., 2019. Multi-crop green LAI estimation with a new simple Sentinel-2 LAI Index (SeLI). Sensors 19 (4), 904.
Peng, Y., Gitelson, A.A., 2011. Application of chlorophyll-related vegetation indices for remote estimation of maize productivity. Agric. For. Meteorol. 151 (9), 1267–1276.
Planet Team, 2018. "Planet imagery product specifications." Planet Labs Inc, Accessed 12/04/2018. https://www.planet.com/products/satellite-imagery/files/Planet_Combined_Imagery_Product_Specs_December2017.pdf.
Planet Team. 2020. "Planet Surface Reflectance Product v2." Planet Labs, Inc, Accessed 18.08.2020. https://assets.planet.com/marketing/PDF/Planet_Surface_Reflectance_Technical_White_Paper.pdf.
Pollock, R., Kanemasu, E., 1979. Estimating leaf-area index of wheat with Landsat data. Remote Sens. Environ. 8 (4), 307–312.
Psomiadis, E., Dercas, N., Dalezios, N.R., Spyropoulos, N.V., 2017. Evaluation and cross-comparison of vegetation indices for crop monitoring from sentinel-2 and worldview-2 images. Remote Sensing for Agriculture, Ecosystems, and Hydrology XIX. International Society for Optics and Photonics.
Qi, J., Chehbouni, A., Huete, A., Kerr, Y., Sorooshian, S., 1994. A modified soil adjusted vegetation index. Remote Sens. Environ. 48 (2), 119–126.
Raun, W.R., Solie, J.B., Johnson, G.V., Stone, M.L., Mullen, R.W., Freeman, K.W., et al., 2002. Improving nitrogen use efficiency in cereal grain production with optical sensing and variable rate application. Agron. J. 94 (4), 815–820.
Rondeaux, G., Steven, M., Baret, F., 1996. Optimization of soil-adjusted vegetation indices. Remote Sens. Environ. 55 (2), 95–107.
Roujean, J.-L., Breon, F.-M., 1995. Estimating PAR absorbed by vegetation from bidirectional reflectance measurements. Remote Sens. Environ. 51 (3), 375–384.
Rouse, J., Haas, R., Schell, J., Deering, D., 1974. Monitoring vegetation systems in the Great Plains with ERTS. NASA SP-351, Washington, DC, pp. 309–317.
Sadeh, Y., Zhu, X., Chenu, K., Dunkerley, D., 2019. Sowing date detection at the field scale using CubeSats remote sensing. Comput. Electron. Agric. 157, 568–580.
Sakamoto, T., Wardlow, B.D., Gitelson, A.A., Verma, S.B., Suyker, A.E., Arkebauer, T.J., 2010. A two-step filtering approach for detecting maize and soybean phenology with time-series MODIS data. Remote Sens. Environ. 114 (10), 2146–2159.
Sripada, R.P., Heiniger, R.W., White, J.G., Meijer, A.D., 2006. Aerial color infrared photography for determining early in-season nitrogen requirements in corn. Agron. J. 98 (4), 968–977.
SUHET, 2015. Sentinel-2 User Handbook. The European Space Agency (ESA), p. 64.
Sun, L., Gao, F., Anderson, M., Kustas, W., Alsina, M., Sanchez, L., et al., 2017. Daily mapping of 30 m LAI and NDVI for grape yield prediction in California vineyards. Remote Sensing 9 (4).
Sun, R., Chen, S., Su, H., Mi, C., Jin, N., 2019. The effect of NDVI time series density derived from spatiotemporal fusion of multisource remote sensing data on crop classification accuracy. ISPRS Int. J. Geo-Inf. 8 (11), 502.
Valderrama-Landeros, L.H., España-Boquera, M.L., Baret, F., 2016. Deforestation in Michoacan, Mexico, from CYCLOPES-LAI time series (2000–2006). IEEE J. Sel. Top. Appl. Earth Obs. Remote Sens. 9 (12), 5398–5405.
Verger, A., Filella, I., Baret, F., Peñuelas, J., 2016. Vegetation baseline phenology from kilometric global LAI satellite products. Remote Sens. Environ. 178, 1–14.
Verrelst, J., Rivera, J.P., Veroustraete, F., Muñoz-Marí, J., Clevers, J.G.P.W., Camps-Valls, G., et al., 2015. Experimental Sentinel-2 LAI estimation using parametric, non-parametric and physical retrieval methods - a comparison. ISPRS J. Photogramm. Remote Sens. 108, 260–272.
Viña, A., Gitelson, A.A., Nguy-Robertson, A.L., Peng, Y., 2011. Comparison of different vegetation indices for the remote assessment of green leaf area index of crops. Remote Sens. Environ. 115 (12), 3468–3478.
Waldner, F., Horan, H., Chen, Y., Hochman, Z., 2019. High temporal resolution of leaf area data improves empirical estimation of grain yield. Sci. Rep. 9 (1), 1–14.
Watson, D.J., 1947. Comparative physiological studies on the growth of field crops: I. Variation in net assimilation rate and leaf area between species and varieties, and within and between years. Ann. Bot. 11 (41), 41–76.
Weiss, M., Baret, F., 2016. S2ToolBox Level 2 Products: LAI, FAPAR, FCOVER, Version 1.1. ESA Contract n° 4000110612/14/I-BG (p. 52): INRA Avignon, France.
Wiegand, C., Richardson, A., Kanemasu, E., 1979. Leaf area index estimates for wheat from LANDSAT and their implications for evapotranspiration and crop modeling 1. Agron. J. 71 (2), 336–342.
Zhu, W., Pan, Y., He, H., Wang, L., Mou, M., Liu, J., 2011. A changing-weight filter method for reconstructing a high-quality NDVI time series to preserve the integrity of vegetation phenology. IEEE Trans. Geosci. Remote Sens. 50 (4), 1085–1094.